

Supporting Information

Reconstruction-induced NiCu-based Catalysts towards Paired Electrochemical Refining

Shanlin Li^{1,2,3}, Peijie Ma², Chunlang Gao², Lijia Liu⁴, Xunlu Wang^{1,3}, Mohsen Shakouri⁵, Roman Chernikov⁵, Kaiwen Wang², Danmin Liu², Ruguang Ma^{6,*}, Jiacheng Wang^{1,3,7*}

1. The State Key Laboratory of High Performance Ceramics and Superfine Microstructure, Shanghai Institute of Ceramics, Chinese Academy of Sciences, Shanghai 200050, China. Email: jiacheng.wang@mail.sic.ac.cn
2. Beijing Key Laboratory of Microstructure and Properties of Solids, Faculty of Materials and Manufacturing, Beijing University of Technology, Beijing 100124, China.
3. Center of Materials Science and Optoelectronics Engineering, University of Chinese Academy of Sciences, Beijing 100049, China.
4. Department of Chemistry, Western University, 1151 Richmond Street, London, ON, N6A5B7, Canada.
5. Canadian Light Source Inc., University of Saskatchewan, Saskatoon, SK, S7N2V3, Canada
6. School of Materials Science and Engineering, Suzhou University of Science and Technology, 99 Xuefu Road, Suzhou 215011, China. Email: ruguangma@usts.edu.cn
7. Hebei Provincial Key Laboratory Nonmetallic Materials, College of Materials Science and Engineering, North China University of Science and Technology, Tangshan 063210, China

Methods

Preparation of NiCu-OH. Nickel foam (NF), carbon paper (CP), or indium tin oxide (ITO) was used as substrate. NF (thickness: 1 mm, size: $1 \times 1 \text{ cm}^2$) was sonicated in 1 M HCl solution for 10 min to remove the oxide layer on the NF surface, and then in water and ethanol for 5 min, followed by drying in air. The co-electrodeposition was carried out in a standard three-electrode electrochemical cell containing NF as the working electrode, a parallel positioned platinum plate as the counter electrode and an Ag/AgCl (3M KCl) as the reference electrode. The electrolyte is composed of 6 mmol $\text{Ni}(\text{NO}_3)_2 \cdot 6\text{H}_2\text{O}$ (1.745 g) and 6 mmol $\text{Cu}(\text{NO}_3)_2 \cdot 3\text{H}_2\text{O}$ (1.45 g) dissolved into 100 ml deionized water. The constant potential electrodeposition was then carried out at -1.0 V (versus Ag/AgCl) at 25°C . The deposition time of NiCu-OH is 300 s. After co-electrodeposition, the NiCu-OH/NF was carefully withdrawn from the electrolyte, rinsed with water and ethanol, and then dried at 60°C overnight.

Preparation of Cu-OH. A one-step hydrothermal method was employed to synthesize the Cu-OH. NF ($3 \times 6 \text{ cm}^2$) was first cleaned as the above. Then, 1.45 g $\text{Cu}(\text{NO}_3)_2 \cdot 3\text{H}_2\text{O}$ was dissolved into 80 ml deionized H_2O . Afterwards, 0.9 g of urea was added, and the above mixture solution was transferred to a stainless-steel Teflon-lined autoclave, and heated in an oven at 140°C for 4 h. After cooling the autoclave to room temperature, the resulting sample was washed by deionized water and ethanol three

times, collected and then dried at 60 °C overnight.

Preparation of Ni-OH. The Ni-OH was also obtained by electrodeposition. The electrolyte is composed of 6 mmol $\text{Ni}(\text{NO}_3)_2 \cdot 6\text{H}_2\text{O}$ (1.745 g) dissolved into 100 ml deionized water. The constant potential electrodeposition was then carried out at -1.0 V (versus Ag/AgCl) at 25°C for 300 s. After electrodeposition, the Ni-OH/NF was carefully withdrawn from the electrolyte, rinsed with water and ethanol, and then dried at 60 °C overnight.

Preparation of NiCuO. The NiCu-OH was then heated in air at 300 °C (heating rate 5°C per min) for 3 h to obtain NiCu oxide (denoted as NiCuO).

Preparation of NiO. The Ni-OH was then heated in air at 300 °C (heating rate 5°C per min) for 3 h to obtain Ni oxide (denoted as NiO).

Material Characterization

The scanning electron microscopy (SEM) images were collected on a field emission scanning electron microscope (FEI Magellan 400L XHR). Transmission electron microscopy (TEM), high-resolution TEM (HRTEM), high angle annular dark-field scanning TEM (HAADF-STEM), and energy-dispersive X-ray spectroscopy (EDS) mapping were taken on FEI-Tecnai-Talos. X-ray diffraction (XRD) measurements were carried out on a Bruker D8 ADVANCE X-ray diffraction diffractometer. X-ray

photoelectron spectroscopy (XPS) measurements were conducted with a Thermo ESCALAB250xi electron spectrometer using Al K α source (1486.6 eV) as a radiation source. The content of dissolved metal ions in the electrolyte was conducted by an inductively-coupled plasma optical emission spectrometry (ICP-OES) on the Agilent 5100. The generated formate at the anode was detected by ion chromatography (IC) (Thermo Scientific Dionex ICS-6000 HPIC).

X-ray absorption fine structure (XAFS) spectra at the Ni K-edge and Cu K-edge were obtained at the Canadian Light Source, beamlines SXRMB and BioXAS, respectively. The samples were pressed into pellets and measured in the transmission mode. For surface sensitive probe, XAFS data was collected as total electron yield (TEY). The data were processed with the ATHENA program for background subtraction, normalization and energy calibration.¹ The extended XAFS (EXAFS) was processed using the IFEFFIT package.² The EXAFS fitting was performed in R-space between 1.0 Å and 3.2 Å (the Fourier transform from k-space was performed over a range of 3.0 to 13.9 Å⁻¹).

In-situ Raman spectra were recorded on a micro-Raman spectrometer (Renishaw) under an excitation of 532 nm laser light under controlled potentials by the CHI 630E electrochemical workstation. The electrochemical operando Raman Cell was provided by the Beijing Scistar Technology Co., Ltd. In addition, the NiCu-OH deposited on ITO was used

as a working electrode. A Pt wire as the counter electrode was rolled to a circle around the cell. Ag/AgCl electrode (sat. KCl) was used as the reference electrode. The *in-situ* Raman spectra were collected under chronoamperometry (I-t) at different potentials in 1.0 M KOH with 0.1 M KNO₃ solution.

Electrochemical measurements

Electrochemical measurements were performed in an H-type cell (H cell) using a CHI 760E electrochemical workstation. A Hg/HgO electrode and a graphite rod were used as the reference electrode and counter electrode, respectively. The as-prepared electrodes were used as the working electrode (1 cm × 1 cm). Fumasep FAB-PK-130 was used as an anion exchange membrane (AEM). All the potentials *vs.* Hg/HgO were converted to the values versus reversible hydrogen electrode (RHE) according to the equation ($E \text{ vs. RHE} = E \text{ vs. Hg/HgO} + 0.924 \text{ V}$). Linear sweep voltammetry (LSV) polarization curves were recorded at a scan rate of 5 mV s⁻¹.

For testing in a flow electrolyzer (manufactured by Gaosunion Co., Ltd., Tianjin, China), we prepared a membrane electrode assembly (MEA) by sandwiching R-NiCu-OH and R-NiCuO electrode between a commercial membrane (Fumasep FAB-PK-130). The MEA was then placed within a custom-designed electrolyzer where 0.1 M KNO₃ and 1 M

KOH as the catholyte and 1 M KOH and 0.1 M glycerol as the anolyte was circulated through cathode and anode, respectively at a flow rate of 20 mL min⁻¹.

Detection of NH₄⁺.

The quantification of NH₄⁺ was conducted with Nessler's reagent as the coloring agent.³ 0.2 mL electrolyte after NO₃RR was first taken out from the cathodic compartment and diluted to 5 mL. Then potassium sodium tartrate solution (500 g L⁻¹, 0.1 mL) was added and thoroughly mixed. In the last step 0.1 mL of Nessler's reagent was added to the above mixture. After being left standing for 20 min, the absorbance at 420 nm was measured by UV-spectroscopy (PG200-Pro back-thinned spectrometer, ideaoptics, China). The obtained value was then fitted to the calibration curve to acquire the corresponding NH₄⁺ concentration.

The NH₄⁺ was calculated as follows:

$$\text{Yield NH}_4^+ = (c_{\text{NH}_4^+} \times V) / (t \times S)$$

The Faradaic efficiency was calculated as follows:

$$\text{Faradaic efficiency} = (8F \times C_{\text{NH}_4^+} \times V) / (M_{\text{NH}_4^+} \times Q)$$

where $c_{\text{NH}_4^+}$ is the mass concentration of NH₄⁺(aq), V is the volume of electrolyte in the cathode compartment, t is the electrolysis time, S is the geometric area of working electrode, F is the Faraday constant (96485 C·mol⁻¹), M_{NH₄⁺} is the molar mass of NH₄⁺, and Q is the total charge passing the electrode.

References:

1. B. Ravel and M. Newville, *J. Synchrotron Radiat.*, 2005, **12**, 537-541.
2. M. Newville, *J. Synchrotron Radiat.*, 2001, **8**, 322-324.
3. X. Deng, Y. Yang, L. Wang, X. Z. Fu and J. L. Luo, *Adv. Sci.*, 2021, **8**, 2004523.

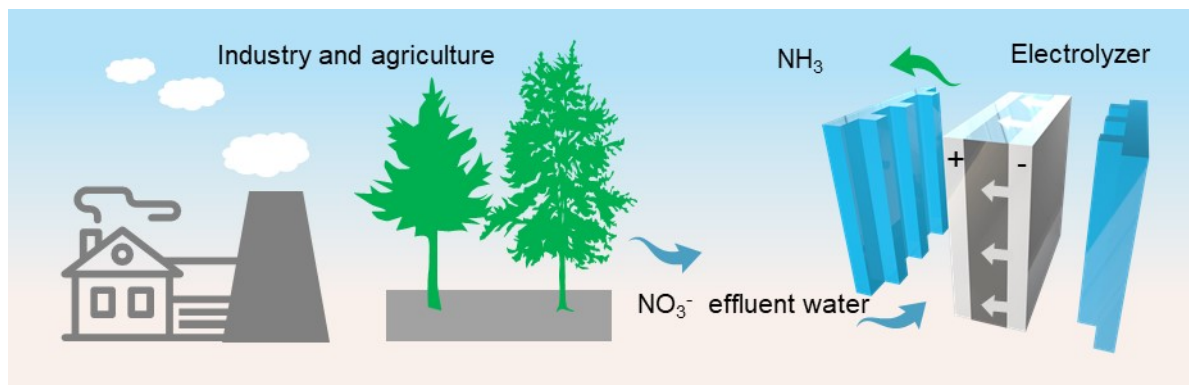


Fig. S1 Schematic showing the conversion of waste NO_3^- (from industry and agriculture) to NH_3 via the electrochemical nitrate reduction reaction (NO_3RR) pathway .

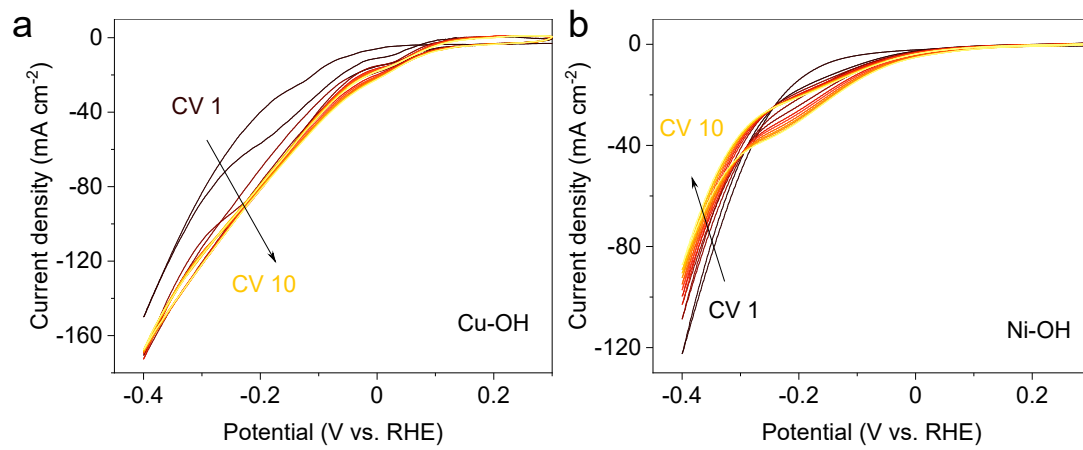


Fig. S2 The first 10 CV cycles for Cu-OH (a) and Ni-OH (b) in 1 M KOH with 0.1 M KNO₃.

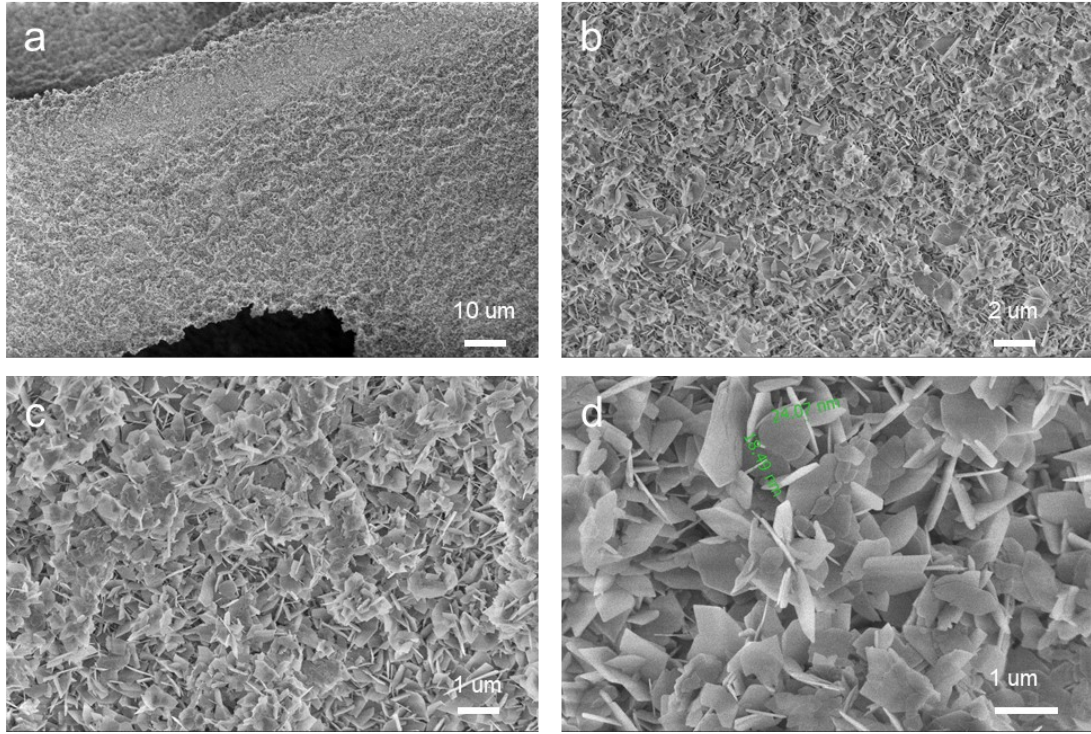


Fig. S3 SEM images of NiCu-OH on NF.

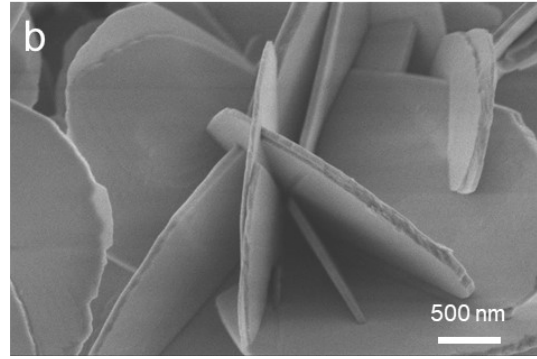
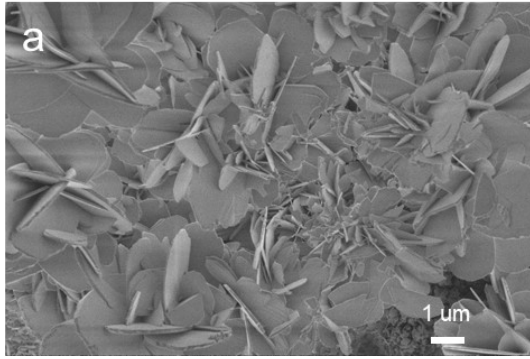


Fig. S4 SEM images of NiCu-OH on ITO.

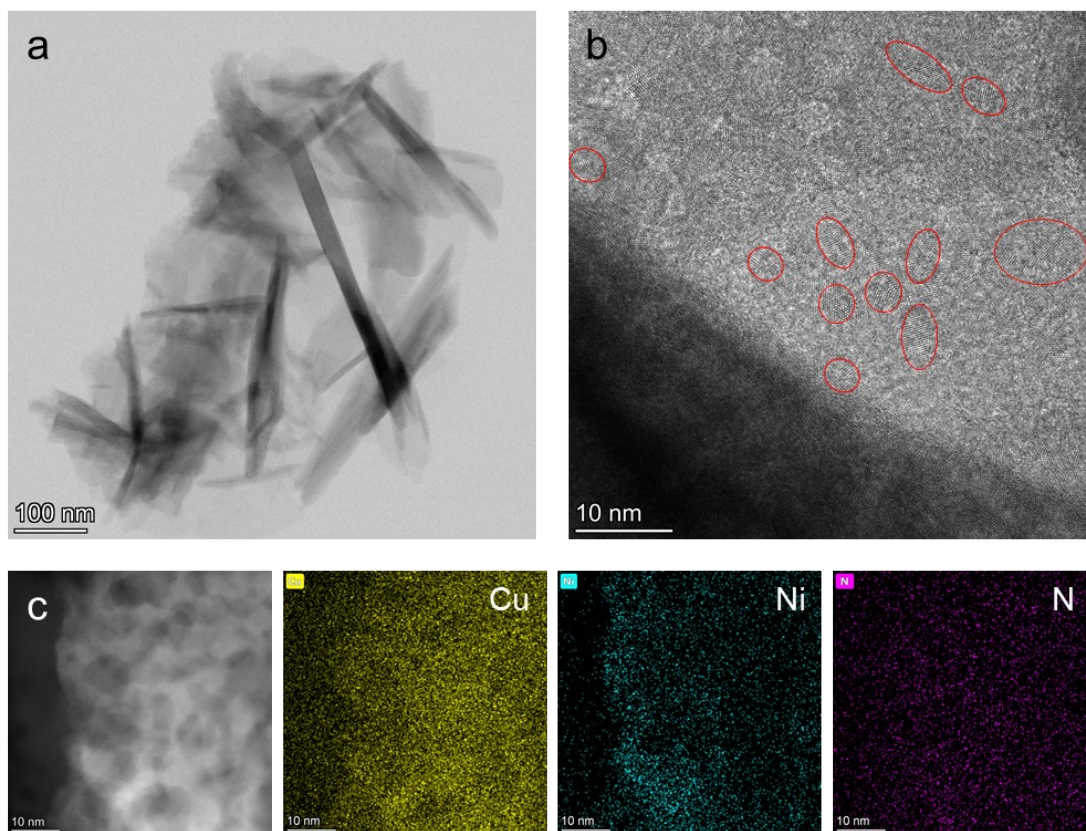


Fig. S5 TEM (a), HRTEM (b), and (c) STEM-HADFF image and element mapping images of NiCu-OH.

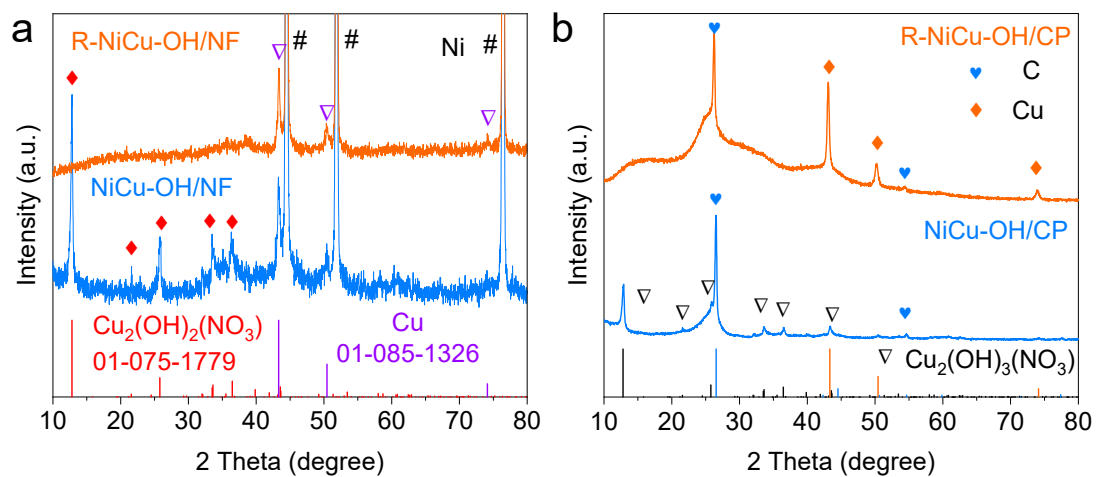


Fig. S6 XRD patterns of NiCu-OH and R-NiCu-OH on nickel foam (NF) (a) and carbon paper (CP) (b).

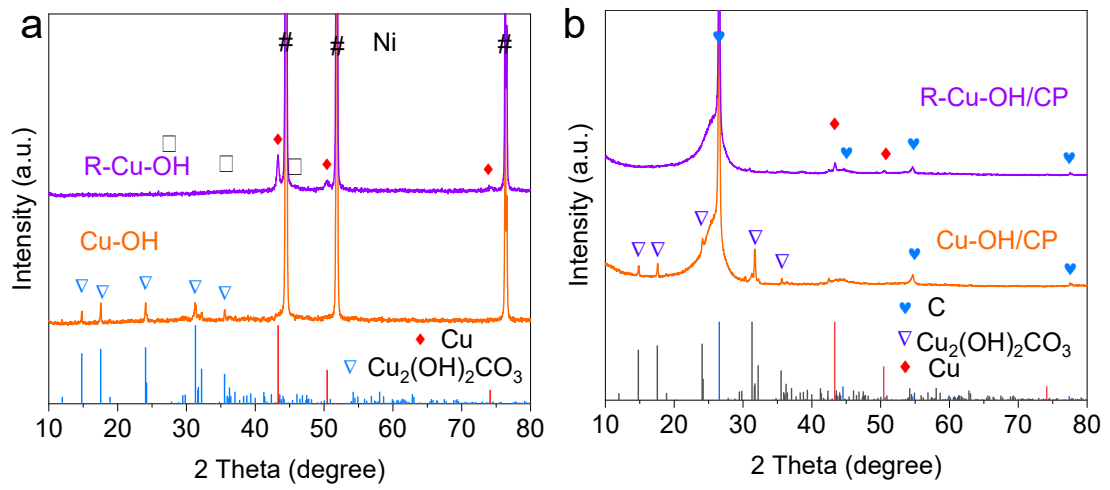


Fig. S7 XRD patterns of Cu-OH and R-Cu-OH on NF (a) and CP (b).

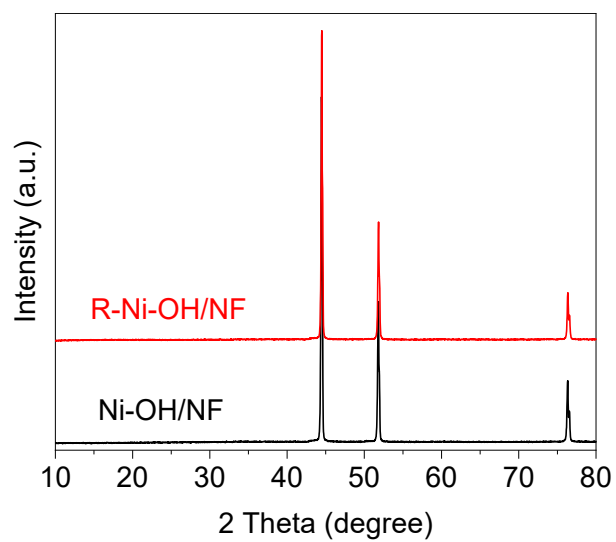


Fig. S8 XRD patterns of Ni-OH and R-Ni-OH on NF.

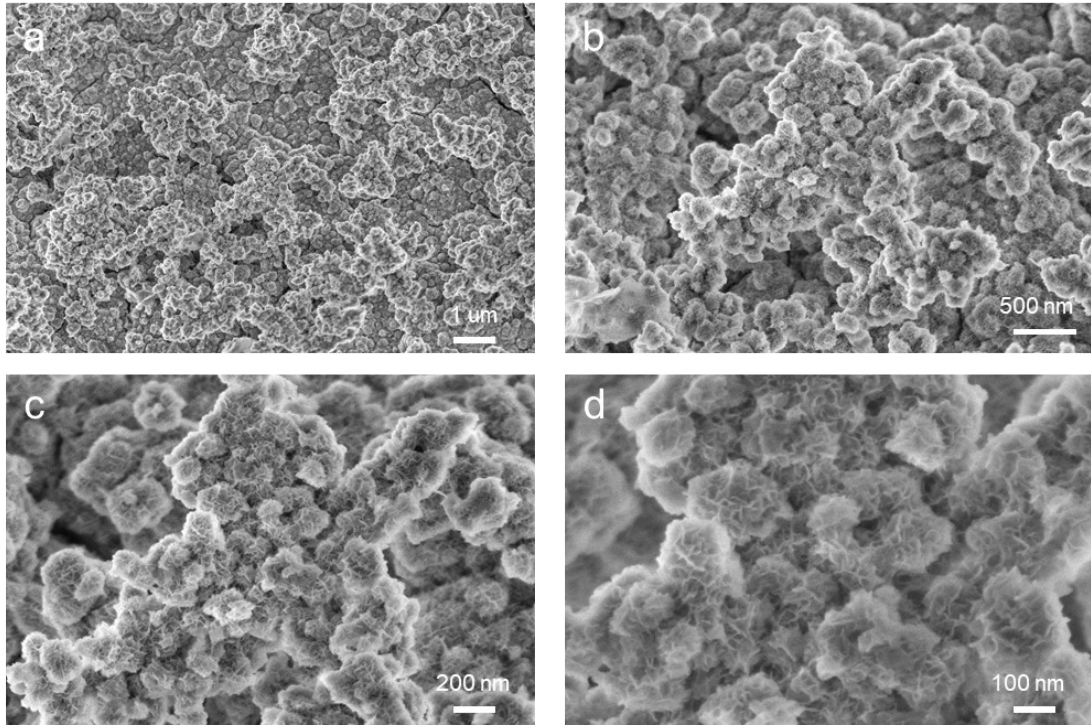


Fig. S9 SEM images of R-NiCu-OH on NF.

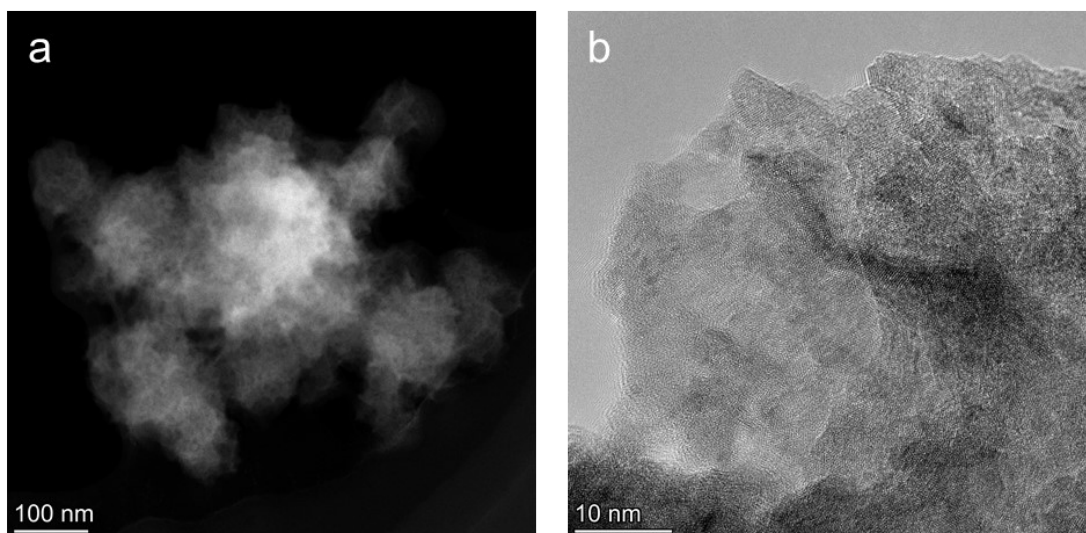


Fig. S10 TEM (a) and HRTEM (b) images of R-NiCu-OH.

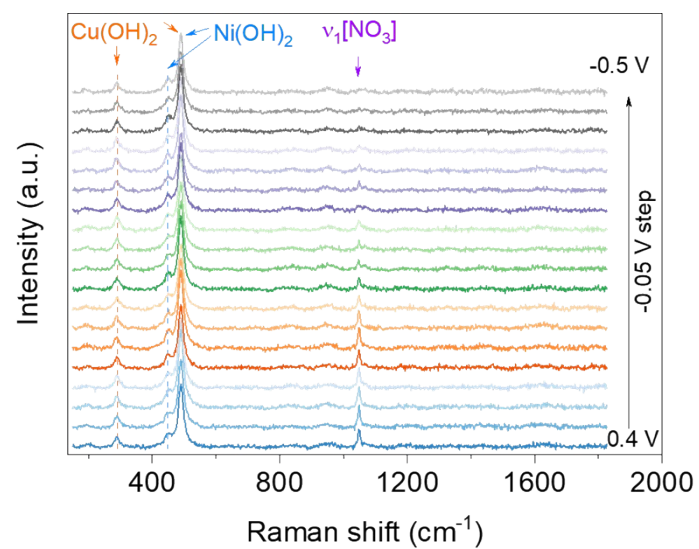


Fig. S11 *In-situ* Raman spectra for NiCu-OH during electrochemical reaction in 1 M KOH with 0.1 M KNO_3 electrolyte.

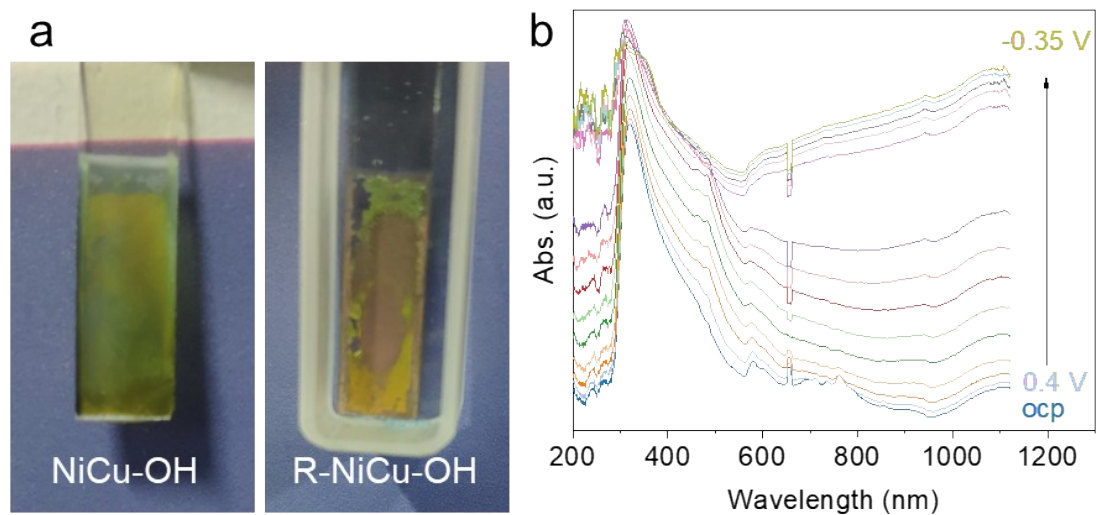


Fig. S12 (a) Digital photos of NiCu-OH and R-NiCu-OH on ITO. (b) *In-situ* UV absorbance of NiCu-OH on ITO during nitrate electroreduction process.

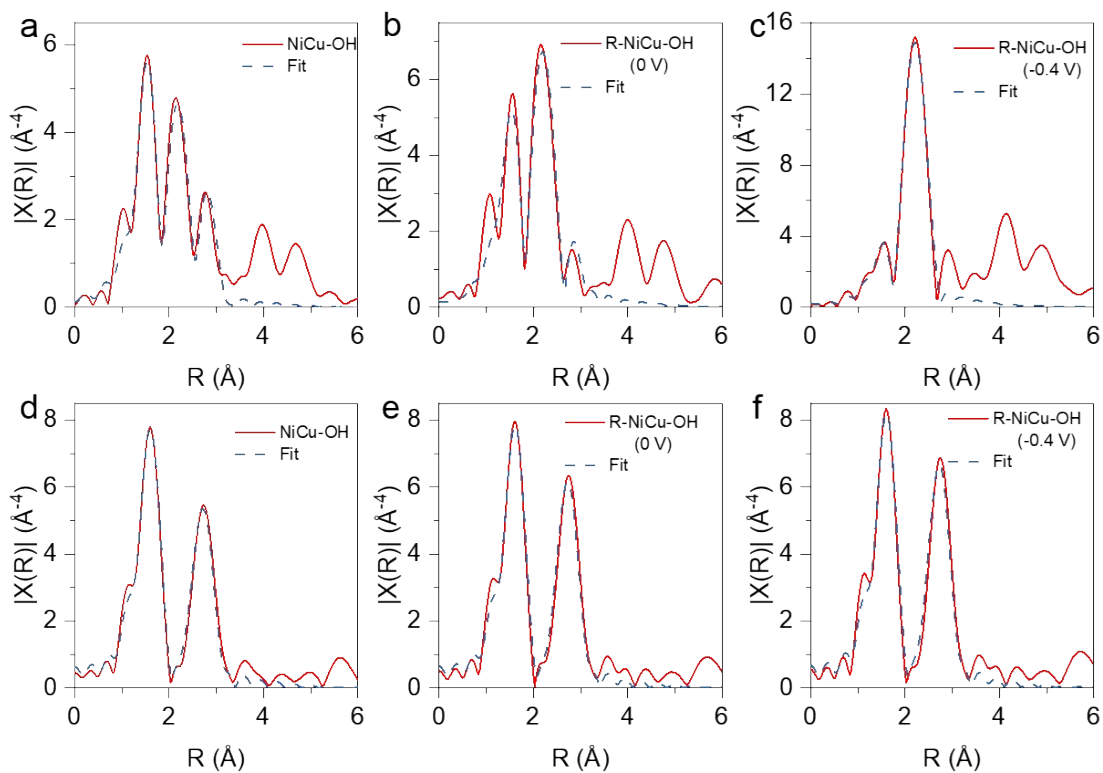


Fig. S13 The Cu EXAFS R-space fitting curves (blue) and the experimental one (red) of NiCu-OH (a), R-NiCu-OH (0 V) (b) and R-NiCu-OH (-0.4 V) (c). The Ni EXAFS R-space fitting curves (blue) and the experimental one (red) of NiCu-OH (d), R-NiCu-OH (0 V) (e) and R-NiCu-OH (-0.4 V) (f).

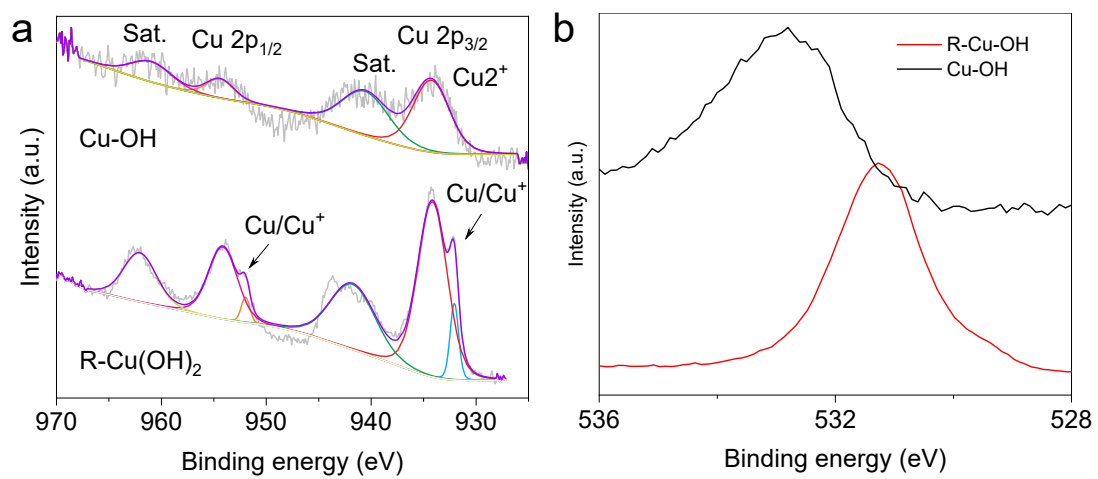


Fig. S14 High resolution XPS of Cu 2p (a) and O 1s (b) in the Cu-OH and R-Cu-OH.

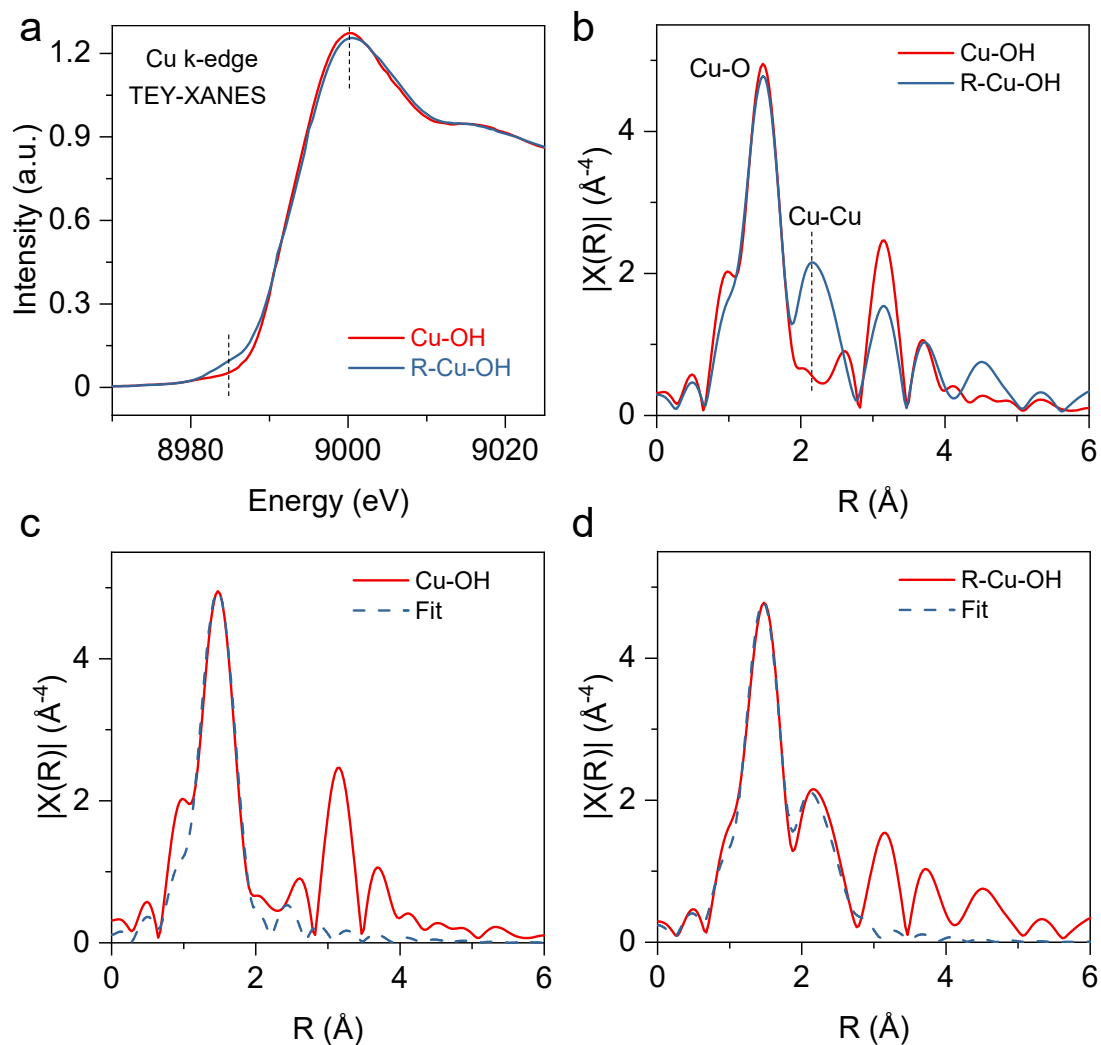


Fig. S15 (a) Cu k-edge TEY-XANES spectra of Cu-OH and R-Cu-OH. (b) Fourier-transforms of k^3 -weight Cu k-edge EXAFS spectra for Cu-OH and R-NiCu-OH. The Cu EXAFS R-space fitting curves (blue) and the experimental one (red) of Cu-OH (c) and R-Cu-OH (d).

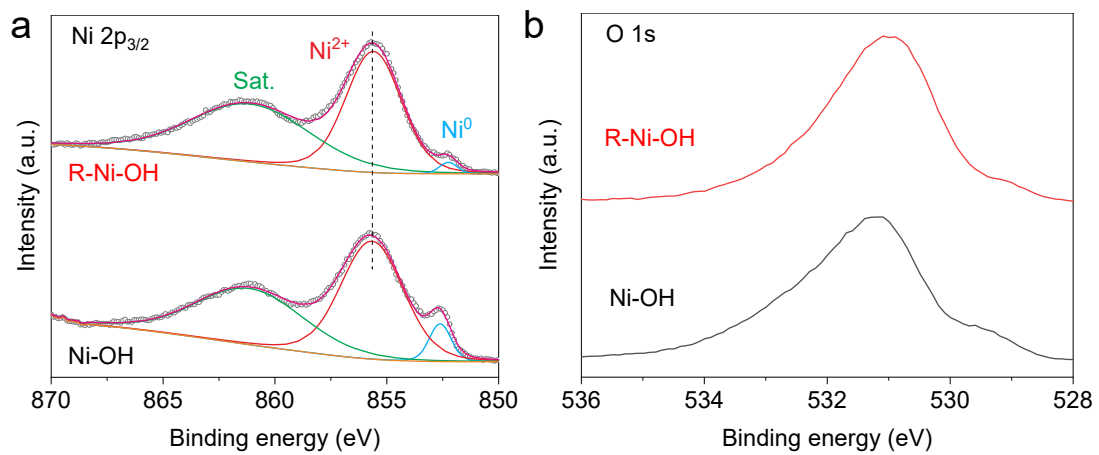


Fig. S16 High resolution XPS of Ni 2p_{3/2} (a) and O 1s (b) in the Ni-OH and R-Ni-OH.

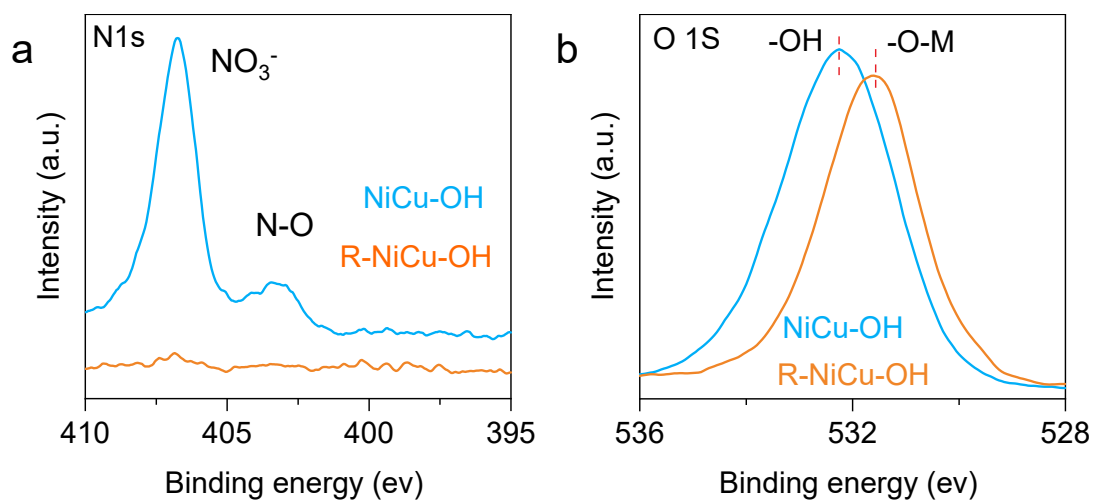


Fig. S17 High resolution X-ray photoelectron spectroscopy (XPS) of N 1s (a) and O 1s (b) in the NiCu-OH and R-NiCu-OH.

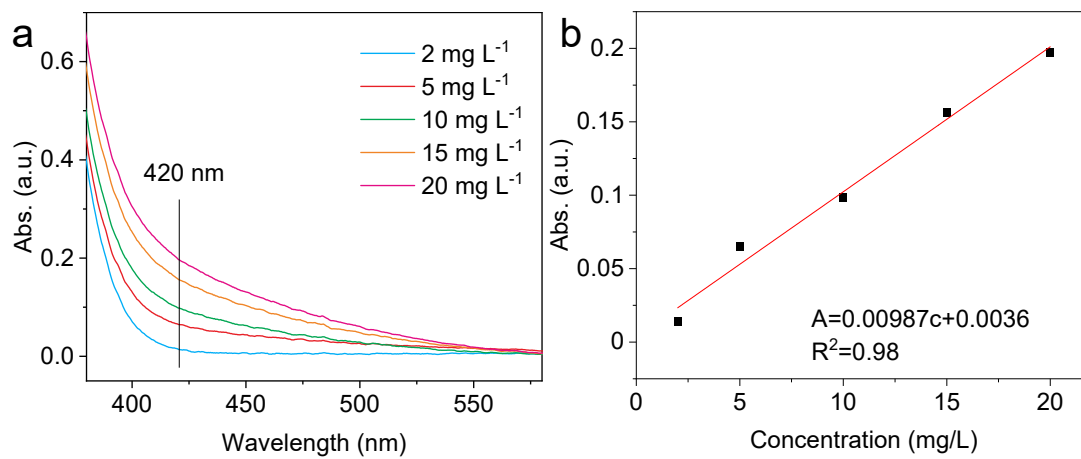


Fig. S18 UV-Vis curves and calibration curves for determining NH_4^+ . 1 mL NH_4Cl standard solutions was diluted to 5 mL for test.

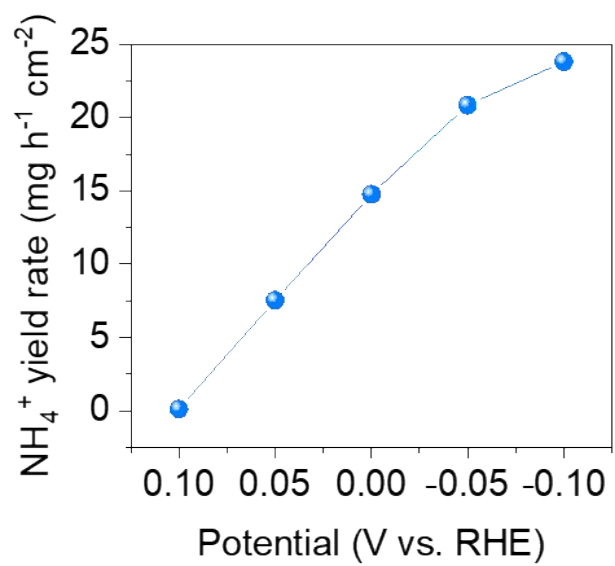


Fig. S19 Ammonia production at various potentials.

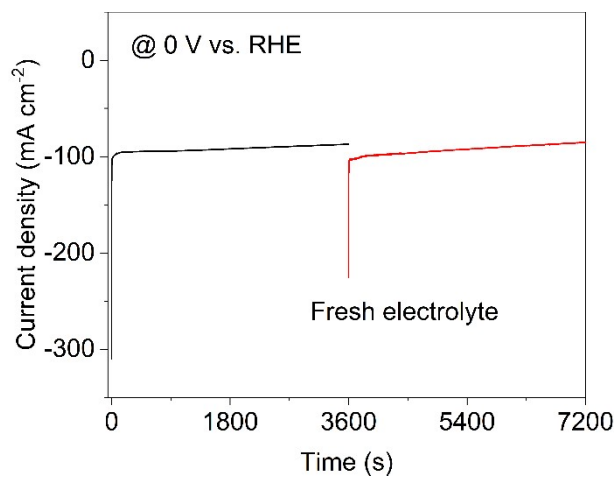


Fig. S20 Chronoamperometry at 0 V vs. RHE for 2 h in 0.1 M KNO₃-containing 1 M KOH as electrolyte. Fresh electrolyte was injected after 1 h to reestablish the initial KNO₃ concentration.

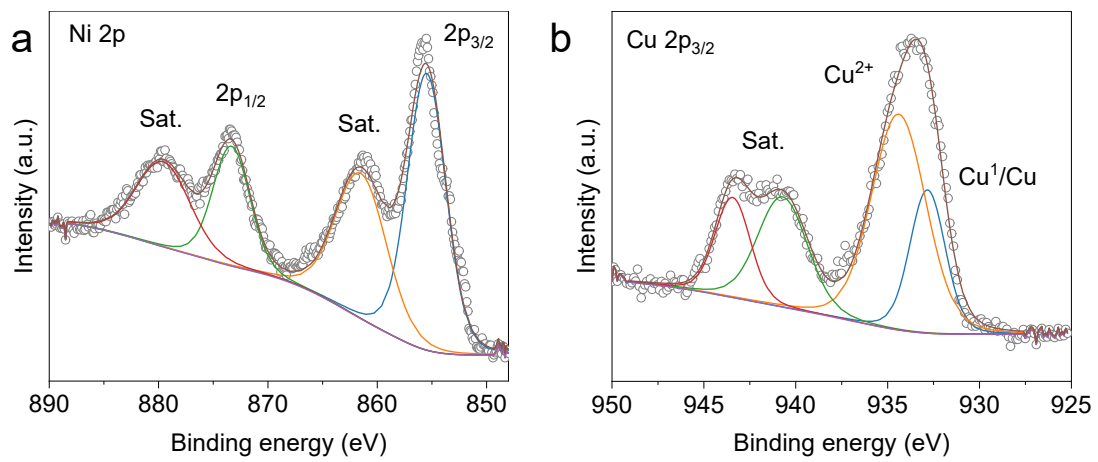


Fig. S21 High resolution XPS of Ni 2p (a) and Cu 2p_{3/2} (b) of R-NiCu-OH after NO_xRR.

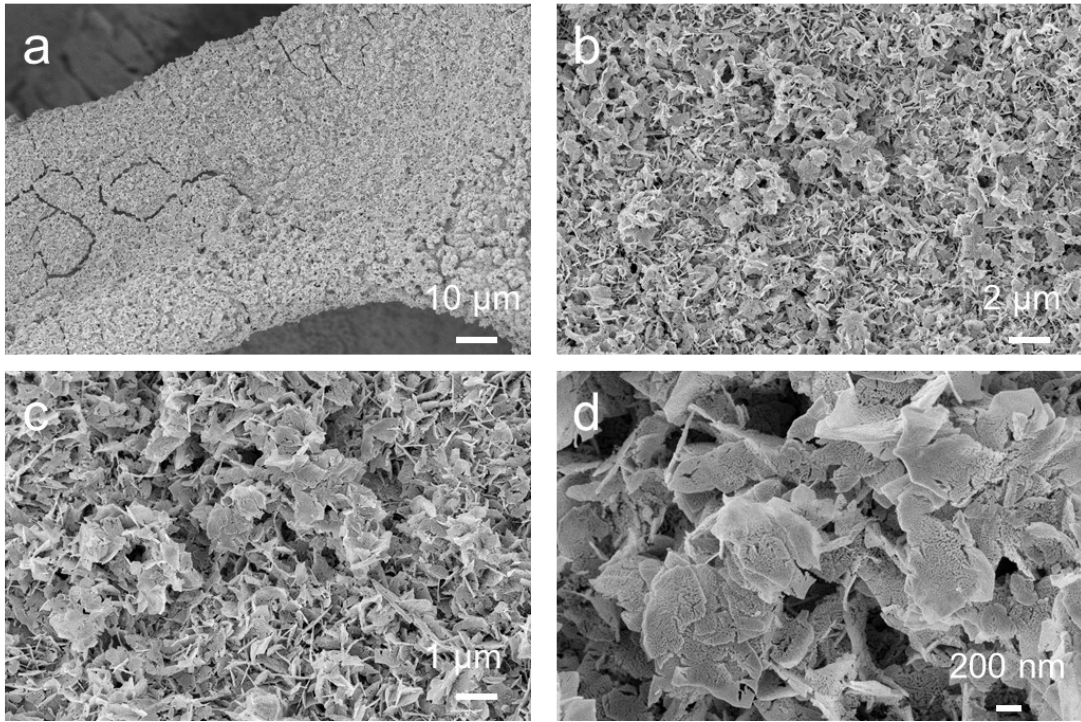


Fig. S22 SEM images of NiCuO on NF.

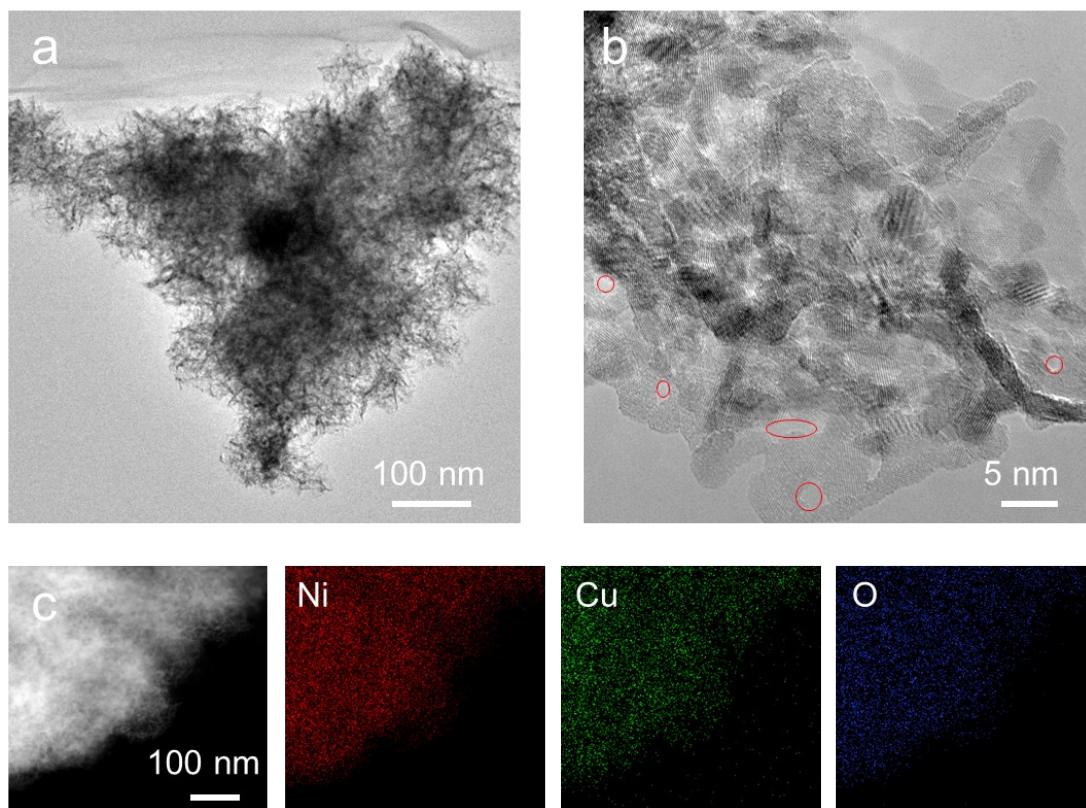


Fig. S23 TEM (a), HRTEM (b), and (c) STEM-HADFF and element mapping images of NiCuO.

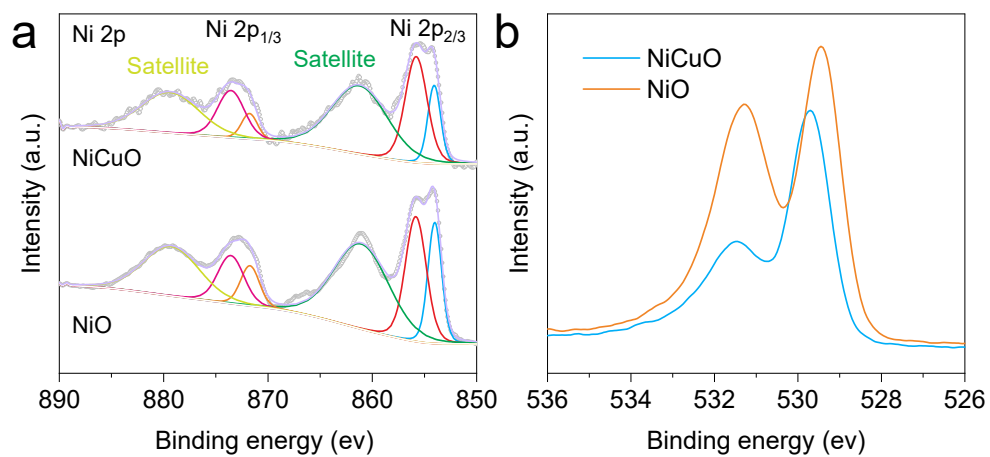


Fig. S24 High resolution XPS of Ni 2p_{3/2} (a) and O 1s (b) XPS of NiCuO and NiO.

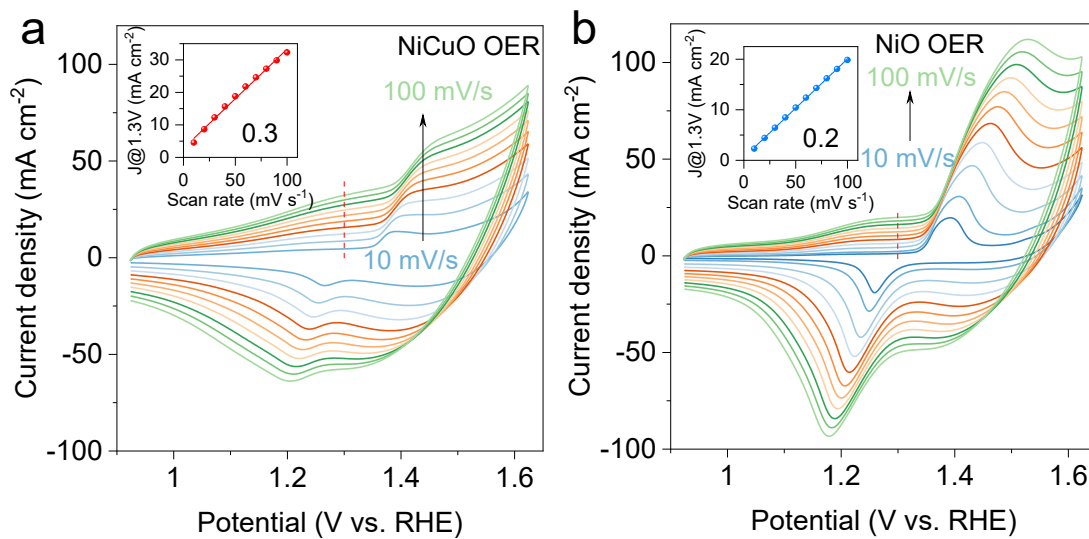


Fig. S25 Cyclic Voltammograms at different voltage scan rates for R-NiCuO (a) and R-NiO (b) in 1 M KOH.

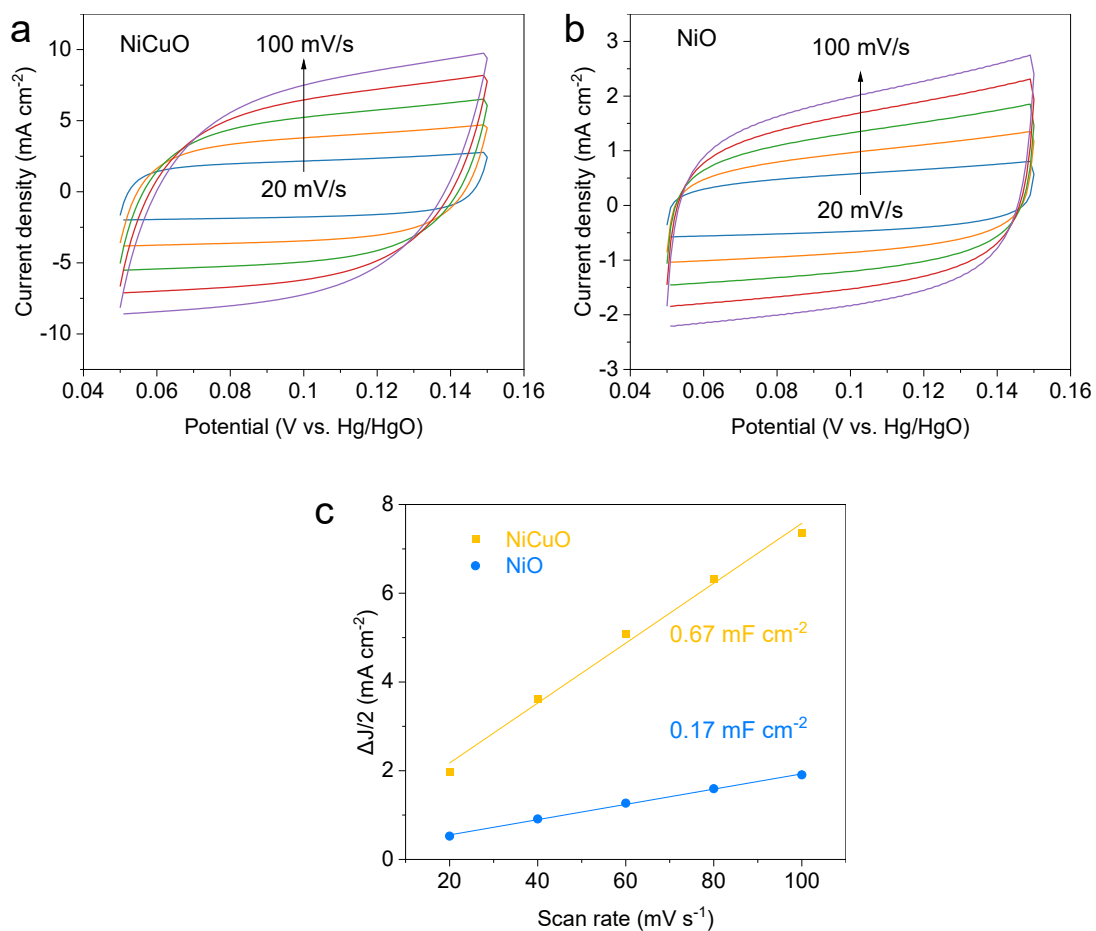


Fig. S26 Double layer capacitance measurements to determine electrochemically active surface area (ECSA) of R-NiCuO and R-NiO in 1 M KOH with 0.1 M glycerol. Cyclic Voltammograms in a non-Faradaic region window at different voltage scan rates for R-NiCuO (a) and R-NiO (b). Currents measured at 0.1 V vs. Hg/HgO as a function of voltage scan rates (c).

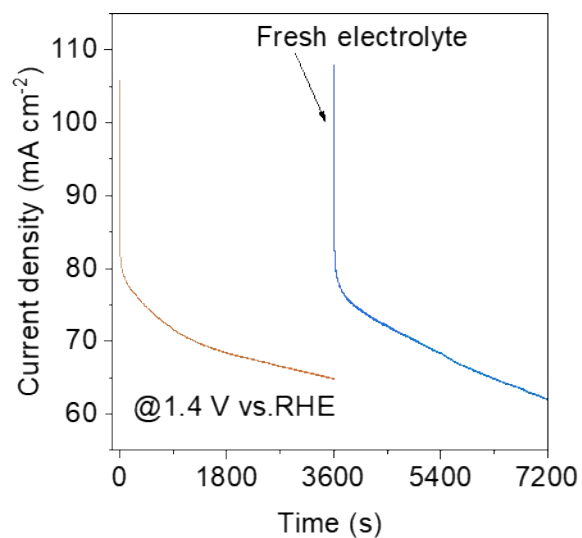


Fig. 27 Chronoamperometry at 1.4 V vs. RHE for 2 h in 0.1 M glycerol-containing 1 M KOH as electrolyte. Fresh electrolyte was injected after 1 h to reestablish the initial glycerol concentration.

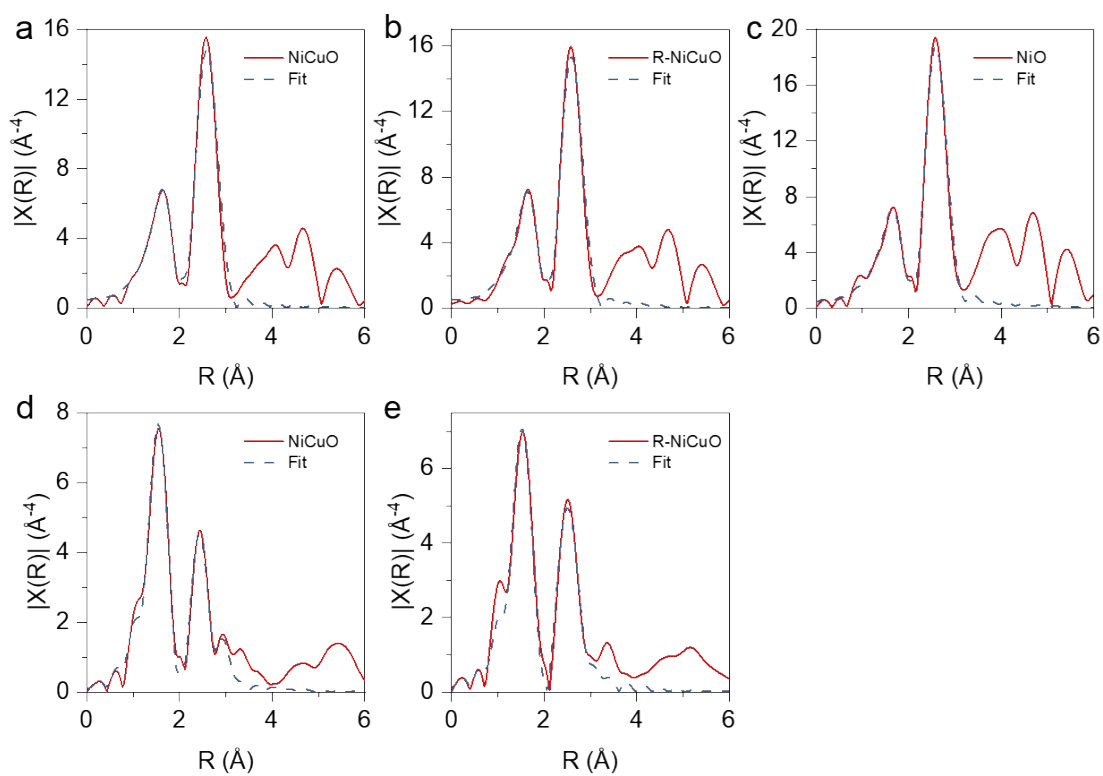


Fig. S28 The Ni EXAFS R-space fitting curves (blue) and the experimental one (red) of NiCuO (a), R-NiCuO (b) and NiO (c). The Cu EXAFS R-space fitting curves (blue) and the experimental one (red) of NiCuO (d), R-NiCuO (e).

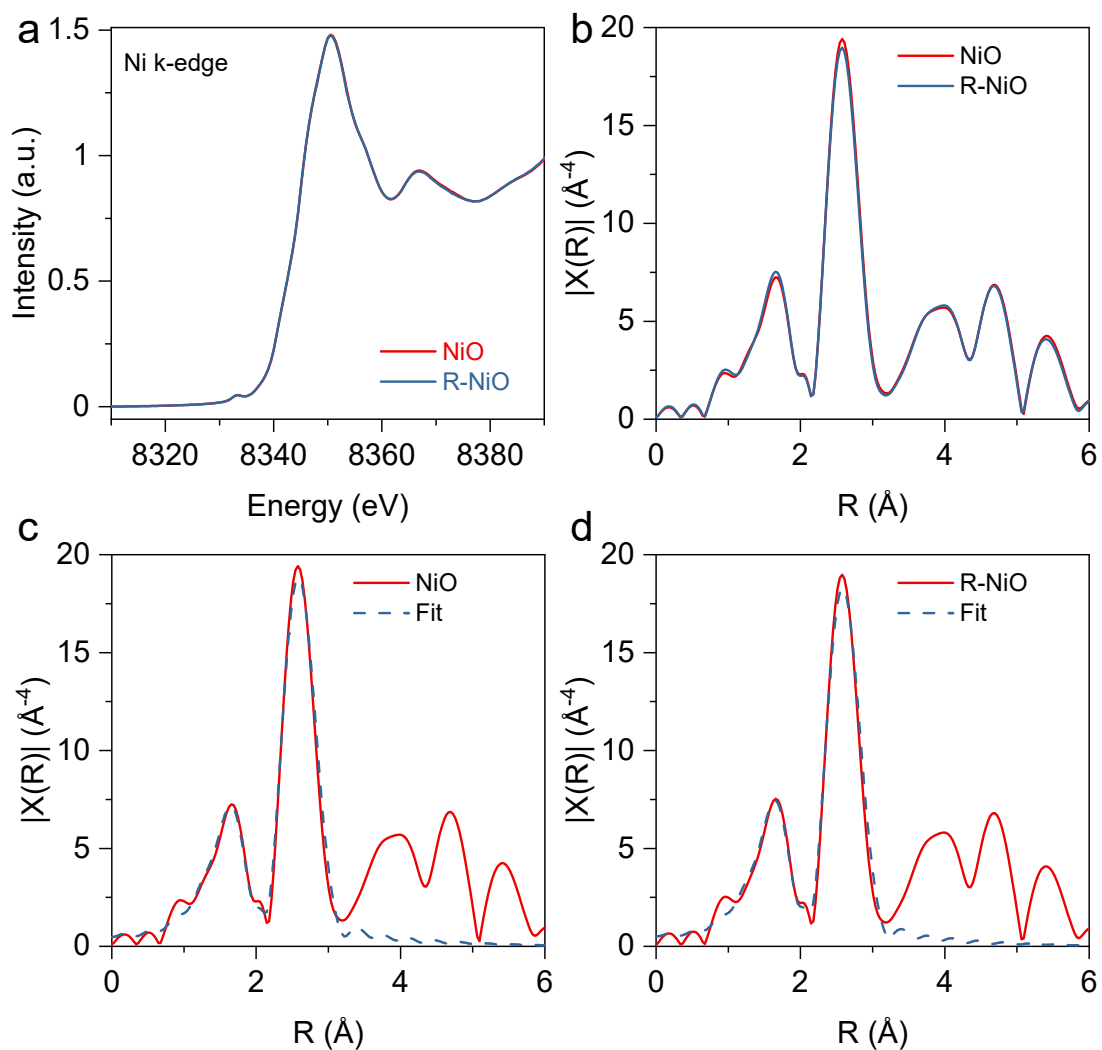


Fig. S29 (a) Ni k-edge XANES spectra of NiO and R-NiO. (b) Fourier-transforms of k₃-weight Ni k-edge EXAFS spectra for NiO and R-NiO. The Cu EXAFS R-space fitting curves (blue) and the experimental one (red) of NiO (c) and R-NiO (d).

Table S1 The standard reduction potentials of metals.

Reaction	Standard potential/V
Ni^{2+}/Ni	-0.257
Cu^{2+}/Cu	0.342

Table S2 Structure parameters extracted from the Cu K-edge EXAFS fittings for NiCu-OH and R-NiCu-OH.

Sample	Path	CN	R (Å)	σ^2	ΔE (eV)
NiCu-OH	Cu-O	2.3	1.951	0.005	-2.651
	Cu-Cu (metal)	2.0	2.566	0.009	
	Cu-Cu (Cu(OH) ₂)	5.1	3.120	0.016	
R-NiCu-OH (0V)	Cu-O	2.4	1.937	0.006	-2.226
	Cu-Cu (metal)	2.5	2.567	0.007	
	Cu-Cu (Cu(OH) ₂)	1.0	3.095	0.007	
R-NiCu-OH (-0.4V)	Cu-O	1.0	1.872	0.004	2.651
	Cu-Cu (metal)	5.4	2.530	0.008	

Table S3 Fitting results of Cu K-edge EXAFS for Cu-OH and R-Cu-OH.

Sample	Path	CN	R (Å)	σ^2	ΔE (eV)
Cu-OH	Cu-O(1)	2.5	1.908	0.006	-1.603
	Cu-O(2)	0.7	2.205	0.005	
R-Cu-OH	Cu-O(1)	2.6	1.909	0.006	-3.753
	Cu-Cu	4.5	2.569	0.015	

Table S4 Structure parameters extracted from the Ni K-edge EXAFS fittings for NiCu-OH , R-NiCu-OH and c--Ni(OH)₂.

Sample	Path	CN	R (Å)	σ^2	ΔE (eV)
NiCu-OH	Ni-O	4.9	2.050	0.007	-2.916
	Ni-Ni	4.8	3.084	0.010	
R-NiCu-OH (0V)	Ni-O	5.0	2.054	0.007	-2.542
	Ni-Ni	5.0	3.088	0.010	
R-NiCu-OH (-0.4V)	Ni-O	5.0	2.053	0.006	-2.623
	Ni-Ni	5.2	3.091	0.009	
c-Ni(OH) ₂	Ni-O	5.8	2.049	0.007	-6.114
	Ni-Ni	6.0	3.084	0.008	

Table S5 Elemental contents of NiCu-OH and R-NiCu-OH from XPS.

Element	NiCu-OH	R-NiCu-OH
C	17.46	32.5
Ni	7.53	7.15
Cu	15.56	13
N	7.04	0.7
O 1s	52.41	46.65

Table S6 Comparing the performance of our synthesized R-NiCu-OH with other reported electrocatalysts for NO₃RR.

Catalysts	Electrolytes	Yield rate	Reference
CuCoSP	0.1M KOH + 0.01M NO ₃ ⁻	1.17 mmol cm ⁻² h ⁻¹ @ -0.175 V vs. RHE	Nat. Commun., 2022, 13, 1129.
Cu ₂ O Ar-40	0.5 M Na ₂ SO ₄ + 200 ppm NO ₃ ⁻	0.0699 mmol h ⁻¹ mg ⁻¹ @ - 1.2 V vs. Ag/AgCl	Applied Catalysis B: Environmental, 2022, 305, 121021.
CuFe-450	1 M KOH + 100 mM HNO ₃	30 mg cm ⁻² h ⁻¹ @ -0.8 V vs. RHE	Chem Catalysis, 2022, DOI:10.1016/j.checat.2022.01.022.
Fe-cyano-R NSs	1 M KOH + 100 mM HNO ₃	1.5 mmol cm ⁻² h ⁻¹ @ -0.6 V vs. RHE	ACS Nano, 2022, 2, 1072–1081.
CoP NAs/CFC	1.0 M NaOH + 1.0 M NaNO ₃	15.44 mol m ⁻² h ⁻¹ @ -0.6 V vs. RHE	Energy Environ. Sci., 2022, 15, 760-770.
CoO _x	0.1 M KOH +100 mM HNO ₃	82.4 mg h ⁻¹ mg ⁻¹ _{cat} @ -0.3 V vs. RHE	ACS Catal., 2021, 11, 15135- 15140.

Fe-PPy SACs	0.1 M KOH + 0.1 M KNO ₃	162.22 μmol cm ⁻² h ⁻¹ @ -0.7 V	Energy Environ. Sci., 2021, 14, 3522-3531.
Cu-NBs- 100	1 M KOH + 0.1 M KNO ₃	650 mmol g ⁻¹ _{cat} h ⁻¹ @ -0.15 V vs. RHE	Energy Environ. Sci., 2021, 14, 4989-4997.
Cu/Cu ₂ O NWAs	0.5 M Na ₂ SO ₄ + 200 ppm NO ₃ ⁻	0.2449 mmol cm ⁻² h ⁻¹ @ -0.85 V vs. RHE	Angew. Chem. Int. Ed., 2020, 59, 5350-5354.
R-NiCu- OH	1 M KOH + 0.1 M KNO ₃	23 mg cm ⁻² h ⁻¹ @ -0.1 V vs. RHE	This work

Table S7 Fitting results of Ni K-edge EXAFS for NiCuO, R-NiCuO and NiO.

Sample	Path	CN	R (Å)	σ^2	ΔE (eV)
NiCuO	Ni-O (NiO)	5.2	2.067	0.008	-2.83
	Ni-Ni (NiO)	11.1	2.975	0.010	
R-NiCuO	Ni-O (NiO)	5.0	2.069	0.004	-2.83
	Ni-Ni (NiO)	10.7	2.978	0.009	
NiO	Ni-O	5.2	2.071	0.008	-3.197
	Ni-Ni	10.3	2.969	0.008	

Table S8 Fitting results of Ni K-edge EXAFS for NiO and R-NiO

Sample	Path	CN	R (Å)	σ^2	ΔE (eV)
NiO	Ni-O	6.0	2.071	0.008	-3.197
	Ni-Ni	12.0	2.969	0.008	
R-NiO	Ni-O	6.0	2.071	0.007	-3.240
	Ni-Ni	12.0	2.969	0.008	

Table S9 Fitting results of Cu K-edge EXAFS for NiCuO and R-NiCuO.

Sample	Path	CN	R (Å)	σ^2	ΔE (eV)
NiCuO	Cu-O	3.1	1.951	0.003	-1.105
	Cu-Cu1	7.1	2.935	0.014	
	Cu-Cu2	1.7	3.125	0.005	
R-NiCuO	Cu-O	3.2	1.951	0.005	-1.923
	Cu-Cu1	11.4	2.967	0.019	
	Cu-Cu2	0.5	3.181	0.003	

Table S10 ICP-OES test of the metal ions in electrolyte and the concentration of formate through IC.

	Concentration (ug/ml)		
	Ni	Cu	Formate
1.3 V	12.8	0.11	5.32
1.4 V	7.15	0.06	14.2
1.5 V	3.99	0.13	20.9
1.6 V	2.15	0.1	28.7
1.7 V	1.43	0.08	31.3

Table S11 Recent NO₃RR electrolyzer.

Anode	Anolyte	Cathode	Catholyte	current	voltage	Reference
R-NiCuO	1 M KOH+0.1 M glycerol	R-NiCu-OH	1 M KOH + 0.1 M KNO ₃	300 mA cm ⁻²	~1.8 V	This work
Ni foam	1 M KOH + 1 M KNO ₃	0D Co	1 M KOH + 1 M KNO ₃	~300 mA	~2 V	Energy Environ. Sci. 14, 6349-6359 (2021).
Ru/Ti O ₂	0.1 M H ₂ SO ₄	pCuO-5	0.05 M KNO ₃ 0.05 M H ₂ SO ₄ 0.05 M KNO ₃	~400 mA cm ⁻²	~2.45 V	Energy Environ. Sci. 14, 3588-3598 (2021).
Ni foam	0.1 M ph-CH ₂ OH + 1 M NaNO ₃ + 1 M NaOH	CoP NAs/CFC	0.1 M ph-CH ₂ OH + 1 M NaNO ₃ + 1 M NaOH	~60 mA cm ⁻²	~1.6 V	Energy Environ. Sci., 2022, 15, 760-770.
Fe/Ni-cyano NSs	1.0 M KOH	Fe/Ni-cyano NSs	0.1 M KNO ₃	~60 mA cm ⁻²	~1.8 V	ACS Nano 2, 1072–1081 (2022).